

Path ensembles for conformational transitions in adenylate kinase using weighted ensemble path sampling

Divesh Bhatt, Daniel M. Zuckerman

Department of Computational Biology, University of Pittsburgh

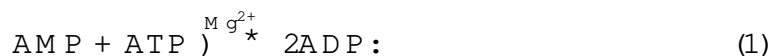
Abstract

We perform first path sampling simulations of conformational transitions of semi-atomistic protein models. We generate an ensemble of pathways for conformational transitions between open and closed forms of adenylate kinase using weighted ensemble path sampling method. Such an ensemble of pathways is critical in determining the important regions of conformation space sampled during a transition. To different semi-atomistic models are used: one is a pure GOM model, whereas the other includes level of residue specificity via use of Miyazawa-Jernigan type interactions and hydrogen bonding. For both the models, we find that the open form of adenylate kinase is more flexible and the transition from open to close is significantly faster than the reverse transition. We find that the transition occurs via the AMP binding domain snapping shut at a fairly fast time scale. On the other hand, the flexible lid domain actuates significantly and the shutting of the AMP binding domain does not depend upon the position of the flexible lid.

1 Introduction

Enzymatic proteins usually show significant differences in the ensemble of apo and holo forms, with large free energy barriers separating the two forms. Due to the large free energy barriers, the fundamental biophysics of the transition between the two forms (such as the transition rates and the transition pathways) are hard to probe computationally. Conventional methods, such as brute force molecular dynamics (MD), are often grossly insufficient.

In this manuscript, we use weighted ensemble path sampling method to study dynamic transition pathways for the *Escherichia coli* adenylate kinase enzymatic protein. This protein catalyzes the reaction between AMP and ATP as follows



email: ddmzz@pitt.edu

Thus, this important enzyme regulates the relative amounts of cellular energetic units. The crystal structure of this enzyme is available in its native apo form in the Protein Data Bank as 4AKE.¹ This structure is shown in Figure 1. In the figure, the blue segments represent the Core, the yellow segment represents the AMP binding domain, and the green segment represents the flexible lid. Upon ligand binding, the enzyme closes. The crystal structure (1AKE)² of the holo form of the enzyme obtained via binding a ligand that mimics both AMP and ATP is shown in Figure 2. Clearly, in the apo form, the enzyme shows an open structure (that we denote as O in this manuscript), and in the holo form, it is closed (denoted by C throughout).

The transitions between the O and the C state (both directions) are studied via employing weighted ensemble path sampling method³ that has been previously been studied to study folding of proteins,⁴ protein dimerization,⁵ and conformational transitions in purely backbone model of calmodulin.⁶

This enzyme has been studied previously via computational methods using both coarse-grained models and fully atomistic simulations. Coarse-grained models used to study transition pathways have, primarily, utilized network models.^{7,8,9,10} In these methods, the fluctuations in proteins are represented by harmonic potentials, and the deformations due to these fluctuations are used to estimate the free energy in the basins (end states and/or multiple basins). Subsequently, a minimum energy path is calculated to characterize the transition. In an interesting amalgamation of such models with atomistic models, Arora and Brooks¹¹ utilized an initial path, obtained using elastic network models, and performed atomistic (with implicit solvent) umbrella sampling molecular dynamics (MD) simulations along the minimum energy path suggested by the network model. Kubitzki and de Groot¹² performed replica exchange MD in the temperature space to enhance conformational sampling of adenylate kinase { and, thereby, observing both O and C conformers. However, the essentially nondynamic nature of replica exchange makes the time ordering of observed conformations in between the two end structures infeasible without heuristic arguments. In addition, fully atomistic MD on the two end structures has also been performed to observe fluctuations in the two ensembles^{13,14} { however, these simulations were not long enough to observe direct conformational transitions, and, hence, did not provide information on the transition pathways.

Due to the inability of fully atomistic MD to observe transitions, coarse-grained models are of immense use. As mentioned above, coarse-grained models have been used to determine transition pathways, there is a lack of knowledge on the ensemble of pathways that contains the essential biophysics of transitions as mentioned above.

Although the so-called minimum energy pathway provides information about the transition, the information is not sufficient { both due to fluctuations within a path "channel", as well as due to possibility of multiple pathways. The goal of this work is to probe the biophysics of transitions with the most detailed models possible that allows for generating an ensemble of pathways. For this purpose we use semi-atomistic models that allow for a comparison of differing level of biochemistry and still allow for sampling of ensemble of pathways using weighted ensemble path sampling.

The manuscript is organized as follows. First, we discuss the two models we used to depict the protein. This is followed by a description of the method to generate the ensemble of pathways. Then, we present results for transitions in both the directions for both the models we used. A few important points are then discussed in the next section. And finally, we present conclusions.

2 Models

We use two semi-atomistic models of the type used previously. In both the models, the backbone atoms are represented in full atomistic details, and only three types of sidechains are considered { alanine, glycine, and proline,¹⁵ with residue specific interactions at a single interaction site at the α carbon. Also, both the models treat the intraresidue interactions explicitly, using OPLS all-atom force field. The intraresidue interactions and the conformations are stored in libraries as discussed in our previous work. The difference in the two models is the level of "chemical" detail as described below. In this path sampling study, the ligand is not modeled.

2.1 Model 1

In the first model, we use a double G ϕ potential for interresidue interactions { with the G ϕ interaction sites at the backbone α carbons. Following Ref¹⁶, contact maps of α carbons for the two crystal structures are generated such that residues less than 8 Å apart are given the same favorable interresidue pair energy, irrespective of the pair type. Clearly, this model does not distinguish between different types of residues at the interresidue level and contacts in both the crystal structures are treated equally.

2.2 Model 2

In this model, we use additional interactions at the inter-residue level. Hydrogen bonding for the backbone-backbone interactions is modeled by electrostatic interactions between the fixed charges of the CO group with the NH group of all residue pair with the O-H distance less than 2.5 Å. Following previous studies that suggest a dielectric constant of 2-5 inside a protein, we use a value of 3. The use of actual charge and distance units in the hydrogen-bonding interactions allow real temperature units in the simulation (instead of merely being in relation to the Go well depth).

We also use Miyazawa-Jernigan (M-J) type residue-residue interactions.^{17,18} Several variants of the original M-J interaction values have been utilized in the literature (such as scaling the M-J interactions energies, as well as shifting)^{19,20} – necessitated due to the fact that M-J values are based on folded protein data and, hence, not directly applicable for unfolded states. We follow suggestion in Ref¹⁹ and mix M-J values of Table V and Table VI (numbering as in the original M-J paper,¹⁷ with updated values as in Ref¹⁸) such that the residue specific interactions are modeled as $x \cdot (\text{Table V}) + (1 - x) \cdot (\text{Table VI})$. The value of x was chosen to be 0.05 such that the residue specific interactions are a significant perturbation of the double Go interactions. To make the crystal structures (meta)stable, we titrated in double Go interactions (same for contacts in both the crystal structures), such that at 300 K, both the crystal structures were (meta)stable. At a Go depth of 400 K, both the structures remained (meta)stable.

2.3 Model 3

The third model employs pure Go interactions as in model 1, however, there is an important difference. In contrast to models 1 and 2, that prescribe same amount of Go strength to contacts in the two crystal structure, the contacts that are present only in the closed form of adenylate kinase are reduced by half as compared to Go strength of other interactions. As is shown shortly, the closed form of adenylate kinase is significantly more stable than the open form using models 1 and 2. Since, we do not model ligands, this can, presumably, be an artifact of models 1 and 2 implicitly accounting for ligand-protein interactions in the closed form, since the closed form crystal structure shown in the Protein Data Bank is obtained in presence of ligands. This additional stabilization of the closed form due to more favorable energy is not offset by entropic cost of ligand binding in models 1 and 2. Thus, model 3 is an

attempt to capture, qualitatively, the effect on the transition pathways of making the closed and the open forms of adenylate kinase more comparable in stability (than allowed in models 1 and 2).

3 Method

We use weighted ensemble path sampling method to generate path ensembles of conformational transitions of adenylate kinase between the open and the closed states. This method was used previously to study protein folding,⁴, protein dimerization,⁵, and conformational transitions of calmodulin using a backbone alpha carbon model.⁶ In this work, we use more detailed models to study the transitions, and evaluate the role of increasing the chemical details on the transitions. Weighted ensemble studies the probability evolution of trajectories in the conformational space using any underlying system dynamics. We use library-based Monte Carlo (LBM-C) method, that we have developed along with other co-workers,¹⁵ to propagate the system using natural system dynamics. No artificial forces are used to direct conformational transitions. The procedure to use weighted ensemble path sampling to study conformational transitions using natural system dynamics is described in detail elsewhere,⁶ here we just describe it briefly. We divide the one dimensional projection of the conformational space (i.e., the RMS from the target structure) into several bins. The RMS is defined as the progress coordinate ξ and is not necessarily the reaction coordinate. The progress coordinate keeps track of the "progress" to the target state and for structures close to the target state, RMS of those structures from the target state are necessarily small. It is also possible to use multidimensional progress coordinates as described by Zhang et al.,⁶ but was not found necessary here.

Several independent simulations are started in the starting conformation and run for a short dynamic step using LBM-C. At the end of a dynamic step, the progress of the simulations along the progress coordinate (i.e., which bin along the progress coordinate a simulation end up after the dynamic step) is noted. At the end of a dynamic step, simulations are split and combined to keep the same number of simulations in each occupied bin, and also to prune simulations that end up in a bin with low probabilities and splitting the ones with high probability. This splitting and combining of simulations is performed as discussed in by Zhang et. al.⁶ In this study, we utilize 25 bins between the two states, with 20 simulations (trajectories) in each occupied bin. The end state is defined as being at a RMS of 1.5Å from the target crystal structure. Due to the degeneracy of the RMS measure, this distance from the

target state was found necessary to be able to capture the target state in all cases. It must be noted that value of flux into either state depends upon the actual definition of the two states. However, the dynamics studied here is Monte Carlo and the fluxes and rates are not in experimentally measurable units. Moreover, a narrow definition of the target states (that we choose in this work), along with the system being far from equilibrium means that the state definition has a negligible effect on the path ensemble. Thus, we do not explore different state definition in this work.

4 Results

4.1 Brute force sampling

Brute force simulations for either structure at several temperatures were performed on Model 1. At $T = 0.75$ (relative to the Gowell depth), both the structures melted, and remained (meta)stable at $T = 0.7$. Thus, for Model 1, all subsequent equilibrium and path sampling simulations are performed at $T = 0.7$.

In a brute force simulation using LBM C with Model 1, tail residues from 201 to 214, that form a helical segment in either structure, are flexible and the corresponding helix unravels at temperatures much lower than stability limit of the rest of the protein in either conformation. We focus on the flexibility of the rest of the protein to monitor conformational transitions. Figure 3 shows the dms from the O structure for the first 200 segments obtained via simulation started from the O structure with a solid line, and dms from C for the first 200 segments obtained via simulation started from C with a dashed line. Small dms value in Figure 3 imply that the structures remain close to the corresponding crystal structure during a simulation. In contrast to the dashed line, the solid line shows larger fluctuations in the dms value implying that the ensemble of conformations obtained upon starting from O is larger. This observation is in accord with previous simulation studies that showed larger fluctuations in the O ensemble.

Deviations from a particular structure in the dms measure do not contain direct information about whether these fluctuations bring the system closer to the other crystal structure. Figure 4 plots the data of Figure 3 as dms from the "opposing" structure. In other words, the solid line represents the dms from C for a simulation started with O, and the dashed line is for dms from O for a simulation started with C. A small ordinate in this figure would imply a transition to the other structure. The large fluctuation for the solid line in Figure 3 around 70 million MC step does

correspond to the starting O structure coming close to the C structure. However, the fluctuations are not large enough to result in a conformational transition, and both the states remain (meta)stable.

Although we show results for $T = 0.7$ here, simulations at lower temperatures also give qualitatively similar results.

Figure 5 shows the dms (of the first 200 residues) from the O structure when simulations are started with O as a solid line, and the dashed line is for the dms from the C structure for simulations started from C. Clearly, there is no transition between the two structures in the timescale of the simulation. Fluctuations in dms for both the structure are similar to the corresponding fluctuations for Model 1. A gain, no transition to the other state is obtained.

4.2 Path Sampling: Models 1 and 2

Figures 6 and 7 show the {carbon distance map of pair of residues in the closed and the open crystal structures, respectively. By construction, both the figures are symmetric about the diagonal (the inter{residue distance near the diagonal is not zero, as suggested by the figures: the white space simply reflects that distances only between pairs that are more than two residues apart are tabulated). A few features of the two structures easily emerge from a comparison of Figures 6 and 7. The inter{residue distances for most of the residue pairs are very similar in the two crystal structures. The major difference are that the distances between residue pairs for residue numbers around 50 and residue numbers around 160 are in close contact in the closed structure. A similar observation can be made for the inter{residue distances between residue pairs for residue numbers around 15 and residue numbers around 130. Referring back to Figures 2 and 1, residues 31 to 60 correspond to the AMP binding domain (yellow) and residues 114 to 164 correspond to the flexible lid (green).

From Figures 6 and 7 it is clear that the structural change that characterizes the transition between the open and the closed structure is fairly straightforward: the lid and the AMP binding domains close, and the rest of the protein remains fairly unchanged. Following Figures 6 and 7, we monitor inter{residue distances between two pairs of residues { residues 56 (GLY) and 163 (THR) and residues 15 (THR) and 132 (VAL). In the closed structure, $d_{56,163}^c = 4.9\text{\AA}$ and $d_{15,132}^c = 6.3\text{\AA}$. On the other hand, in the open structure, $d_{56,163}^o = 23.6\text{\AA}$ and $d_{15,132}^o = 17.8\text{\AA}$. Thus, the distances between the core and the lid domain are monitored, along with distances between two residues in the lid and the AMP binding domains.

4.2.1 Transition from Open State to Closed States

Figure 8 plots the WE results for probability fluxes obtained into the closed state for both the models. The "time" axis is merely the number of snapshots (where one snapshot contains 2000 LBM C steps). In both cases, the fluxes reach linear regimes indicating that the observed transitions are not merely due to initial fast trajectories. Additionally, Model 2 (with a level of residue specific chemistry) has a smaller flux into the closed state than Model 1. Residue specific interactions are expected to roughen up the energy landscape along the transition path(s), thus the slowing of transition dynamics is not unexpected. However, it is not possible to separate out the effect of the inclusion of residue specific chemistry on the relative free energies of the open state basin and the barrier height.

Figures 9{12 shows the projection of individual trajectories onto the $d_{15,132}$ and $d_{56,163}$ plane obtained via WE for open to close transition. The filled circle shows the closed structure, whereas the filled diamond is for the open structure. The corresponding open circles and diamond are representative of fluctuations in the ensemble of closed and open structures, respectively, of adenylate kinase. Structures in the equilibrium ensemble for either conformation are divided into Voronoi bins based on the distance on the $d_{15,132}$ { $d_{56,163}$ plane from several randomly chosen reference structures. The structures in each bin with the largest distance from the corresponding crystal structure are, then, shown as the representative ensembles in Figures 9{12. The dashed line represents the trajectory of a particular transition from the open to the closed structure. Although the trajectories arrive at the target state with different weights, the ones shown in the figures above are obtained after a simple resampling with the largest weight and, thus, represent trajectories that arrive with relatively large probabilities.

The relatively larger spread of structures representing the open ensemble compared to the closed ensemble reflects the larger fluctuations in the open structures depicted previously in Figure 3. In all the three panels, the trajectories spend a significant amount of time near the equilibrium ensemble for each state. Another point to note is that although the two crystal structures show a large difference in $d_{15,132}$, the fluctuations in the ensemble for the open and the closed states (especially, the large fluctuations in the ensemble for the open conformation) allow the distance between the lid domain and the core to sample values relevant to either ensemble. On the other hand, the distance between the AMP binding domain and the flexible lid, $d_{56,163}$, does not show an overlap in the two ensembles. In all the trajectories, the transition through the region with values of $d_{56,163}$ intermediate between the two ensembles is

fairly rapid. The flexible lid undergoes large fluctuations in the open state, and the transition to the closed state is accomplished via the AMP binding domain snapping close on a much smaller time scale.

Given the significant difference between pathways suggested above, we classify the path according to whether the AMP binding domain snaps shut after the flexible lid relaxes to the closed form (as in Figure 12 { Pathway 1) or the AMP binding domain snaps shut before the flexible lid gets close to the CORE (as in Figure 11 { Pathway 2). Mathematically, we define a trajectory to follow Pathway 1 if it last visits the region $d_{56,163} > 9.0 \text{ \AA}$ and $d_{15,132} < 8.5 \text{ \AA}$ before going to the closed state (equivalently, for close to open transition, this is so if a trajectory first enters this region after leaving the closed state). On the other hand, a trajectory follows Pathway 2 if it last visits the region $d_{56,163} < 5.5 \text{ \AA}$ and $d_{15,132} > 10.0 \text{ \AA}$ before going to the closed state. All the resampled paths can be sorted into either of the two pathways. We find that for open to closed transition using Model 1, approximately 60% of the resampled trajectories follow Pathway 2 (the AMP binding domain snaps shut when the flexible lid is away from the Core region - Figure 11).

Further, we look at a few intermediate structures for these two paths. Figure 16 shows four intermediates along the path shown in Figure 11. Clearly, the AMP binding domain and the flexible lid come closer together before the flexible lid closes. On the other hand, Figure 17 shows four intermediates along the path given by Figure 12. The closing of the flexible lid, followed by snapping shut of the AMP binding domain is clear visible in the figure. As both Figures 16 and 17 show, the rest of the protein (i.e., the CORE region) maintains a stable shape during the transformation.

A similar qualitative picture is obtained for Model 2 that incorporates a level of residue specificity. Figures 13 and 14 plot resampled trajectories from the open to the closed structure using Model 2. Again, the symbols have the same meaning as in Figure ?? (except that open circles and diamonds represent the fluctuations in the closed and the open states, respectively, of adenylylate kinase obtained using Model 2). In accordance with smaller domain fluctuations obtained in either state using Model 2, the fluctuations in the two distance coordinates in either state are smaller in Figures 13 and 14 than in Figures 9{12. This leads to a more pronounced separation between the two states for Model 2. A trajectory, again, spends a significant amount of time sampling $d_{56,163}$ values corresponding to the equilibrium ensemble. The transition from the open to closed structure primarily takes place by the AMP binding domain snapping close to the lid domain on a much shorter time scale. Depending upon the relative positions of the flexible lid and the core, the completion of transi-

tion requires further adjustment of the flexible lid relative to the core. For this model 35% of the resampled trajectories follow Pathway 1 and the remaining 65% follow Pathway 2 for the open to close transition.

4.2.2 Transition from Closed State to Open State

In addition, we study reverse transitions { from the closed state to the open state. Figure 15 shows the flux into C as a function of "time" for both the models (solid line for Model 1 and dashed line for Model 2). Compared to Figure 8 for the transition from the open to the closed state, the flux into state B is several orders of magnitude lower. This observation quantifies the observed larger fluctuations in the open state ensemble. Additionally, flux into the open state for Model 2 with residue specific chemistry is higher than for Model 1, despite the expected roughening up of the energy landscape along the transition path(s). This can be, perhaps, due to changing of relative free energy barriers between the closed state basin and the barrier(s).

For C to O transition using either model, we obtain results very similar to the O to C transition { the flexible lid fluctuates in the closed state, and this is followed by the AMP binding domain snapping open on a relatively fast time scale. For both the models, successful trajectories appear to follow only Pathway 2 for close to open transition. A possible reason for not observing the other transition path for the reverse transition is that the transients for Pathway 1 in the reverse direction are very large. This is not surprising because the reverse reaction rates, shown in Figure 15, are very small for both models 1 and 2.

4.3 Path Sampling: Model 3

The slow transition from close to open suggests that both model 1 and 2 result in the free energy of the closed structure being significantly lower than that of the open structure. As discussed above, this called for the use of Model 3, that lowers the favorable energy for contacts present only in the closed state { to account for free energy asymmetry induced by not including the ligand explicitly. As shown in Figure 18, that although the flux in the open to close direction in Model 3 is higher than in the close to open direction, the difference between the fluxes in the two directions is much less than that for models 1 and 2. The increased rate from close to open direction implies that the relative stability of the closed and the open structures is reduced from models 1 and 2.

The pathways for conformational transitions in either direction are very similar

to the ones presented above. Both the pathways are observed for transition from the open to the close direction, as well as in the close to open direction. In contrast to models 1 and 2, transitions from close to open overcome the transients faster and it is easier to obtain Pathway 1 in this direction (contrast with models 1 and 2). For the open to close direction, approximately 50% of resampled trajectories follow each path. In comparison with models 1 and 2, Pathway 1 is more pronounced for Model 3.

5 Discussion

5.1 Models

In this manuscript, we have used three different models for protein. Two are based purely on structure (Go model) and the other includes some level of residue specificity via Miyazawa-Jernigan interactions, as well as hydrogen bonding energies and Ramachandran propensities. In Model 2, the other energy terms are smaller than the Go energy, however, are significant perturbations. This model is designed to be able to capture some level of biochemistry. From the results, transition pathways are not significantly affected by the inclusion of this level of residue specificity. Pure MJ interactions, derived from a databank of protein crystal structures, emphasize the native crystal structures heavily at the cost of extended structures. This required the use of rescaling MJ interactions as has been previously done in the literature.

It is possible to use other models for residue specific interactions. However the coarse-grained level description that we utilize still requires a significant Go-type interaction to stabilize the two physical states.

As noted above, we did not consider the ligand in our path sampling simulations. The inclusion of ligand is expected to influence the observed rates. We have plans for modeling ligand via mixed models that include all-atom ligands and binding sites, with a coarse-grained picture for the rest of the protein. Such an explicit inclusion of ligands, with the corresponding degrees of freedom of the unbound ligands in the open form can reduce the dependence on arbitrary scaling of closed structure-only contacts as is done in Model 3. Such a study with explicit ligands will require a higher dimensional progress coordinates to use in weighted ensemble: one coordinate for protein structure (as is done in this work), and a second (or further) coordinates for distance between ligands and the protein.

5.2 Steady state

One of the main reasons that models 1 and 2 were unable to show transitions in the close to open direction is that the transients in that direction are very large. This results in steady state being hard to achieve. Currently, we are working on developing methods that allow steady state to be reached faster without perturbing the natural dynamics of the system.

5.3 CPU time

The results shown for Model 1 in the open to close direction took approximately one week of single CPU time (3 GHz intel processor, with 2 GB memory). A lot more snapshots were obtained in the close to open direction, and these required 3-4 weeks of single CPU time. The results for model 2 were obtained using approximately the same time as model 1 (in the two directions). For model 3, the close to open transition was not much harder to obtain than the open to close transition, and the results shown required approximately a week of single CPU time.

5.4 Comparison with brute force

Although comparison of WE with brute force simulations has been discussed previously,⁶ we briefly mention the reason behind observing transitions faster using WE than with brute force.

In principle, several long brute force simulations can also provide full transition pathways. In fact, if the WE simulation protocol is chosen such that only one trajectory is kept at an occupied bin (instead of 20, as we do in our implementation), then the WE method is exactly equivalent to a single brute force simulation. However, the ability of WE to monitor small progress probabilities due to splitting of trajectories is lost. Such a splitting of trajectories in regions of space that occur with low probability in between the two end states greatly enhances the chances of observing transitions. In addition, combination of trajectories in region of high probability keeps the number of brute force simulations at each step low (although splitting and combining to keep the number of trajectories/bin to 20 occurs in each bin, as well as to statistically remove low weight trajectories and split high weight ones).

To elaborate further, we consider a thought WE simulation in which n bins are occupied. Further, each bin has the same number, m , of trajectories. Thus, the total number of short brute force simulations required at each step is nm . Now we

imagine that a trajectory in each bin has a multiple $q(> 1)$ of the probability of a trajectory in the next bin, and that all trajectories in a particular bin have equal weight. Such a scenario, when converted into an equivalent fully brute force scenario (no combination/splitting) where there are m trajectories in the final occupied bin, requires that there be $m + m q + m q^2 + \dots + m q^{n-1} = m (q^n - 1)/(q - 1)$ simulations (due to all trajectories in a fully brute force implementation having equal weight) to correspond to the same progress (i.e., m trajectories in bin n). As $q > 1$, this sum can be significantly larger than nm .

However, the above discussion contains only a partial picture { fully brute force simulations are eventually not expected to be as slow as suggested above. This is because each fully brute force simulation gives independent trajectories, whereas the splitting procedure in WE results in correlated trajectories. Due to these correlations, it is hard to establish number of independent trajectories in a WE implementation. Nevertheless, the low "rates" obtained for the C to O transition (Figure 15) suggest that the time required to observe such a transition using pure brute force is very large, whereas WE shows several transition events.

6 Conclusions

We apply weighted ensemble path sampling to generate ensemble pathways for conformational transition between open (apo) and closed (holo) forms of adenylate kinase. To enable the study of path ensembles, the use of coarse-grained models was required. No additional driving force was used to enable the transitions { natural system dynamics was preserved. We use three different models for the protein. Two of the models employ pure (double) G ϕ interactions based on the two crystal structures in the data bank. In one of these pure G ϕ models, native contacts of the two structures (open and close) have the same energy { well depth. The other pure G ϕ model has closed only contacts scaled by half. The use of these two models was prompted by the fact that we do not model ligand explicitly { and the model with all G ϕ well depths equal implicitly includes stabilization due to ligand and overemphasizes the stability of the closed form. For pure G ϕ model with all well depths equal, the transitions from open to close are significantly faster than from the close to the open state. Reducing the well depth of closed only contacts reduces the stability of closed form, and, as expected, the transition rate in the close to open state is increased. Additionally, another model with some amount of residue specificity developed that included Miyazawa-Jernigan type interactions, as well as hydrogen bonding, and Ra-

machandran propensities { along with G o interactions (with all well depths equal). The inclusion of residue speci city did not change results signi cantly. For all the three models, the transition from open to close state showed two dominant pathways: in one the AMP binding domain snaps shut and the exible lid subsequently gets closer to the Core domain, in the other pathway, the AMP domain shuts after the exible lid gets close to the Core region of the protein. For the reverse direction, the model with pure G o with contact strength for closed only contacts halved, the transition rate is fast enough to allow probing time scales beyond the transients { and we obtain the same two dominant pathways.

References

- [1] Muller, C.W., G.Schlauderer, J.Reinstein, and G.E.Schultz. 1996. *Structure*. 4:147{156.
- [2] Muller, C.W., and G.E.Schultz. 1992. *J.Mol Biol*. 224:159{177.
- [3] Huber, G.A., and S.Kim. 1996. *Biophys. J.* 70:97{110.
- [4] Rojnuckarin, A., S.Kim, and S.Subramanian. 1998. *Proc. Natl. Acad. Sci.* 95:4288{4292.
- [5] Fisher, E.W., A.Rojnuckarin, and S.Kim. 2000. *J.Molec. Struct.(Themochem)*. 529:183{191.
- [6] Zhang, B.W., D.Jasnow, and D.M.Zuckerman. 2007. *Proc. Natl. Acad. Sci.* 104:18043{18048.
- [7] Maragakis, P., and M.Karplus. 2005. *J.Mol Biol*. 352:807{822.
- [8] Whitford, P.C., O.Miyashita, Y.Levy, and J.N.Onuchic. 2007. *J.Mol Biol*. 366:1661{1671.
- [9] Chennubhotla, C., and I.Bahar. 2007. *PLoS Comput. Biol*. 3:1716{1726.
- [10] Chu, J.W., and G.A.Voth. 2007. *Biophys. J.* 93:3860{3871.
- [11] Aora, K., and C.L.Brooks. 2007. *Proc. Natl. Acad. Sci.* 104:18496{18501.
- [12] Kubitzki, M.B., and B.L.de Groot. 2008. *Structure*. 16:1175{1182.
- [13] Pontiggia, F., A.Zen, and C.Micheletti. 2008. *Biophys. J.* 95:5901{5912.
- [14] Henzler-Wildman, K.A., V.Thai, M.Lei, M.Ott, M.WolfWatz, T.Fenn, E.Pozharski, M.A.Wilson, M.Karplus, C.G.Hubner, and D.Kern. 2007. *Nat.* 450:838{844.
- [15] Mamonov, A.B., D.Bhatt, D.J.Cashman, Y.Ding, and D.M.Zuckerman. 2009. 113:10891{10904.
- [16] Zuckerman, D.M. 2004. 108:5127{5137.
- [17] Miyazawa, S., and R.L.Jernigan. 1985. *Macromolecules*. 18:534{552.

- [18] Miyazawa, S., and R. L. Jernigan. 1996. *J. Mol. Biol.* 256:623{644.
- [19] Jernigan, R. L., and I. Bahar. 1996. *Curr. Op. Struct. Biol.* 6:195{209.
- [20] Gan, H. H., A. Tropsha, and T. Schlick. 2000. *J. Chem. Phys.* 113.

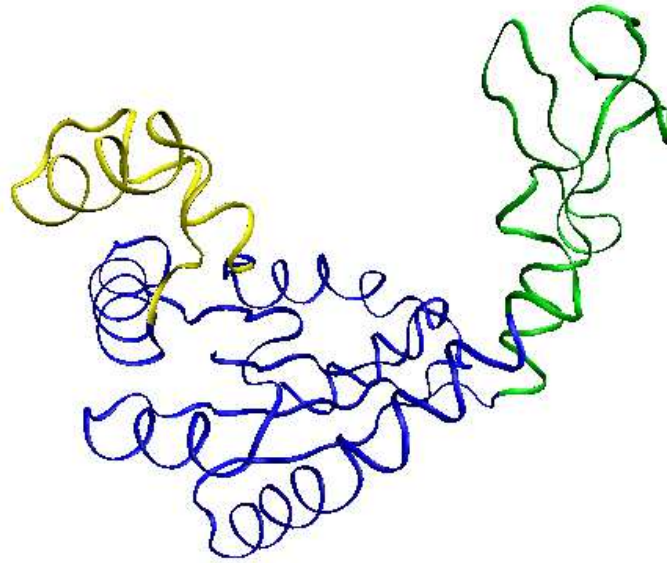


Figure 1: Apo (O) form of adenylate kinase. The blue segment represents the core of the protein, the yellow segment is the AMP binding domain, and the green segments is the flexible lid.

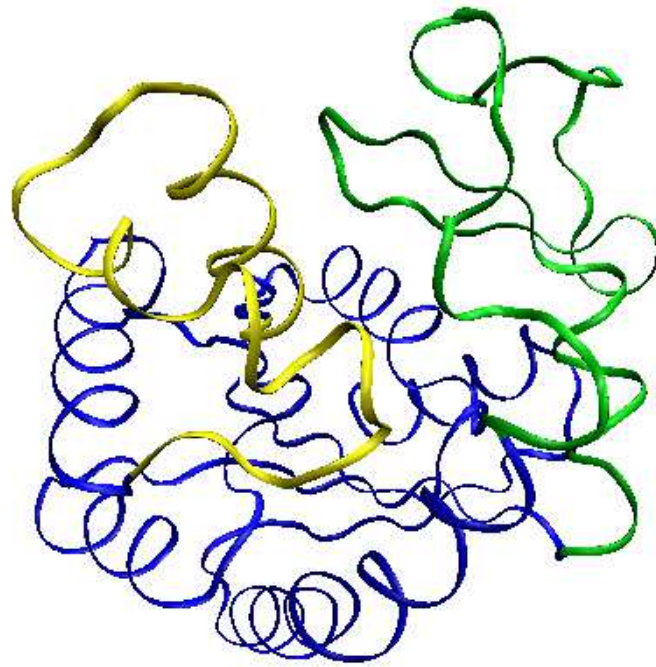


Figure 2: Holo (C) form of adenylate kinase. The blue segment represents the core of the protein, the yellow segment is the AMP binding domain, and the green segments is the flexible lid.

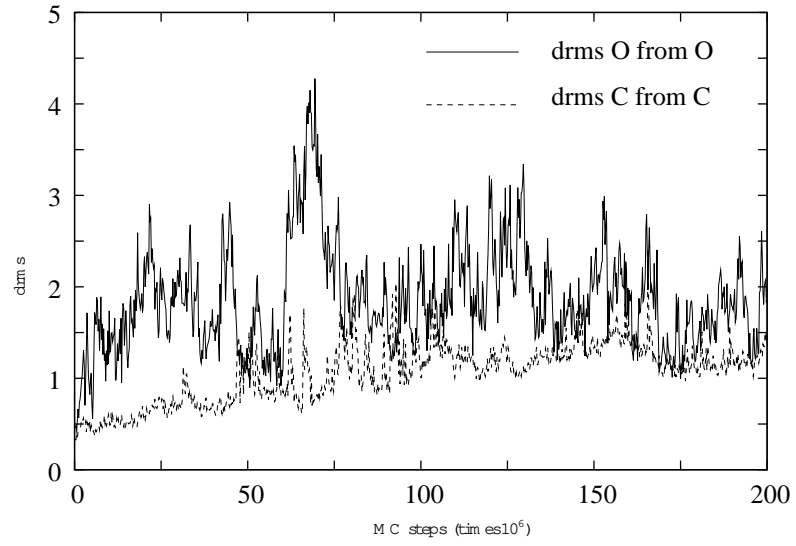


Figure 3: Drms for Model 1 for two simulations from the corresponding starting crystal structure. The solid line gives the drms from O crystal structure of a simulation started from O, whereas the dashed line gives the drms from the C crystal structure of a simulation started from C.

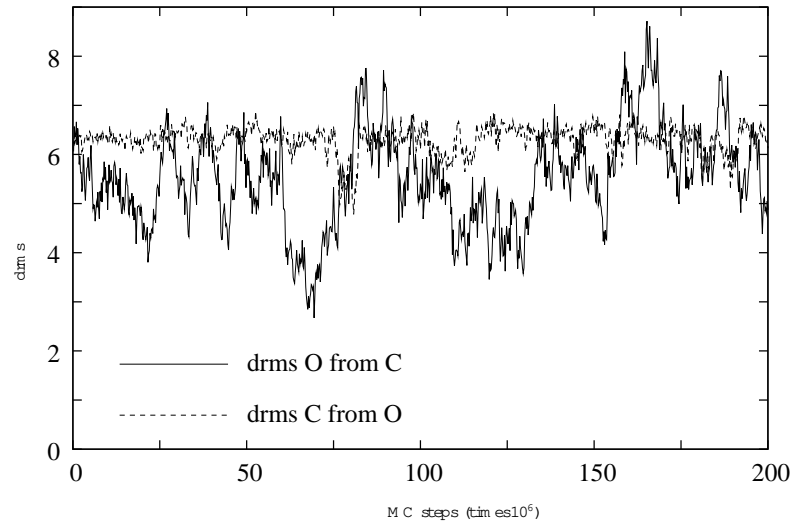


Figure 4: Drms for Model 1 for two simulations from the opposing crystal structure. The solid line gives the drms from C crystal structure of a simulation started from O, whereas the dashed line gives the drms from the C crystal structure of a simulation started from O.

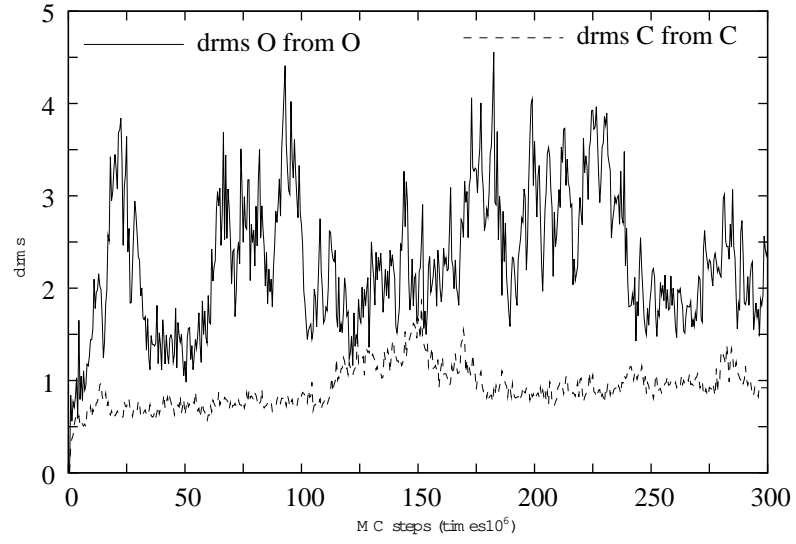


Figure 5: D rms for Model 2 for two simulations from the corresponding starting crystal structure. The solid line gives the d rms from O crystal structure of a simulation started from O, whereas the dashed line gives the d rms from the C crystal structure of a simulation started from C.

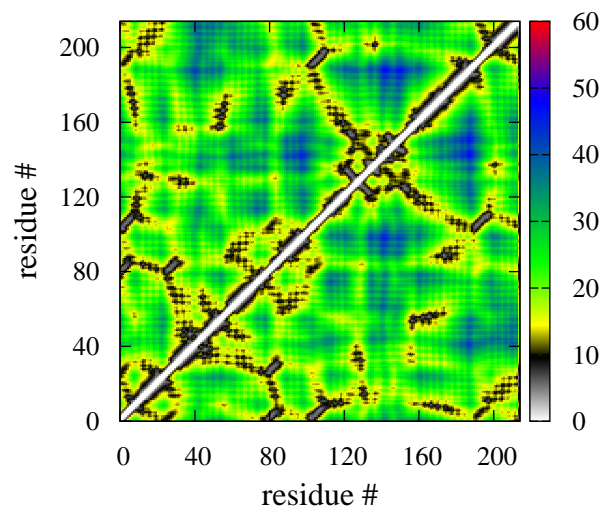


Figure 6: Map of the inter-residue distances for the C crystal structure. The map is, by definition, symmetric about the diagonal. The white space on the diagonal just implies that we do not calculate distances between residue pairs less than 2 residues apart along the chain.

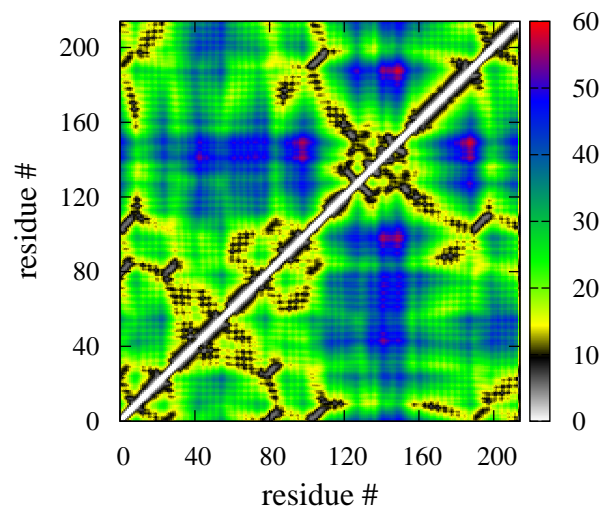


Figure 7: Map of the inter-residue distances for the O crystal structure. The map is, by definition, symmetric about the diagonal. The white space on the diagonal just implies that we do not calculate distances between residue pairs less than 2 residues apart along the chain.

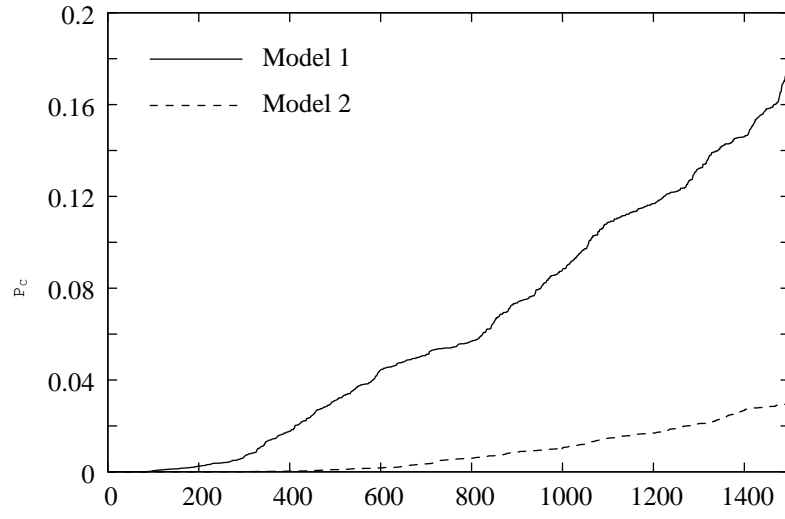


Figure 8: Probability P_C into the C state as a function of WE snapshots (each snapshot is 2000 LBM C steps). The solid line is for Model 1, whereas the dashed line is for Model 2.

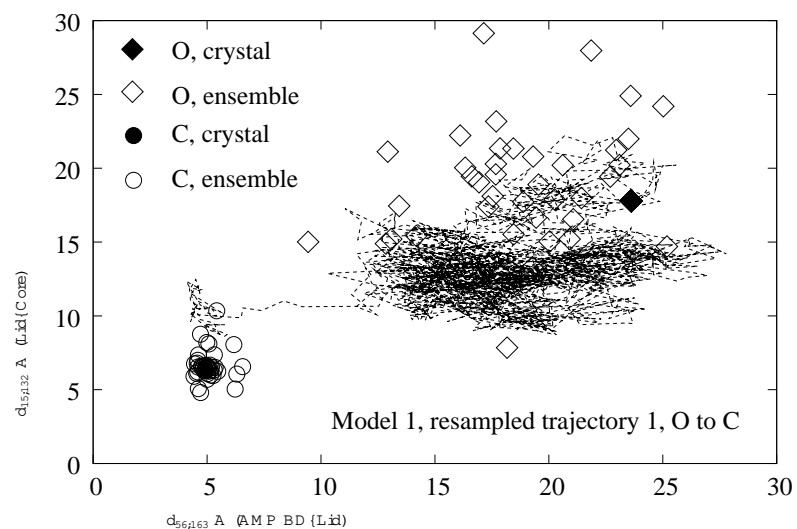


Figure 9: A resampled trajectory for the O to C transition obtained using Model 1 is shown via interresidue distance between pair of residues in the core and the flexible lid (ordinate) versus the distance between pair of residues in the AMP binding domain and the flexible lid (abscissa).

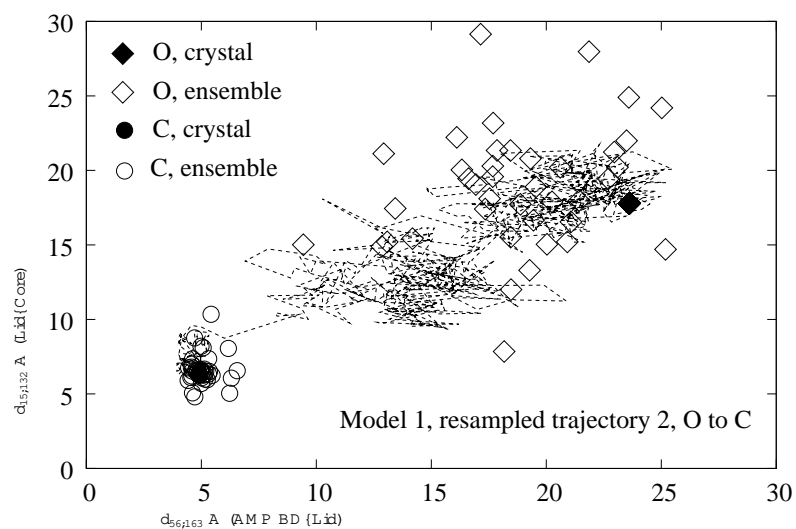


Figure 10: A resampled trajectory for the O to C transition obtained using Model 1 is shown via interresidue distance between pair of residues in the core and the flexible lid (ordinate) versus the distance between pair of residues in the AMP binding domain and the flexible lid (abscissa).

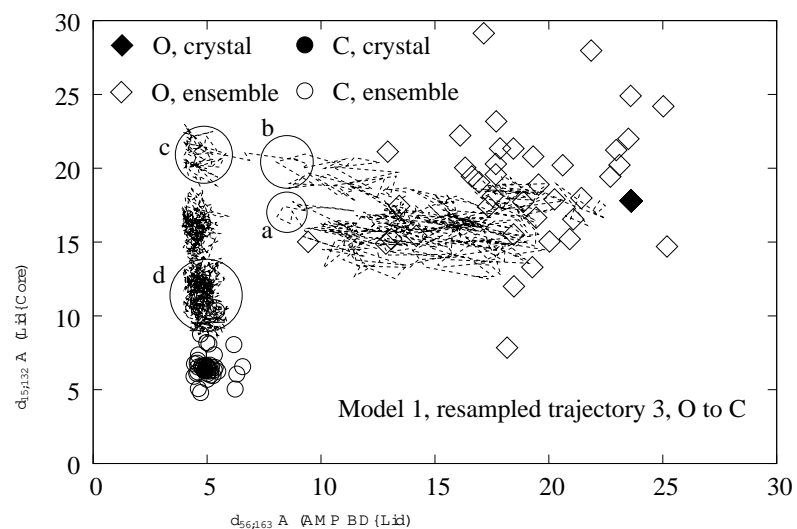


Figure 11: A resampled trajectory for the O to C transition obtained using Model 1 is shown via interresidue distance between pair of residues in the core and the flexible lid (ordinate) versus the distance between pair of residues in the AMP binding domain and the flexible lid (abscissa). The circles and associated numbers represent the representative structures that are depicted in Figure 16.

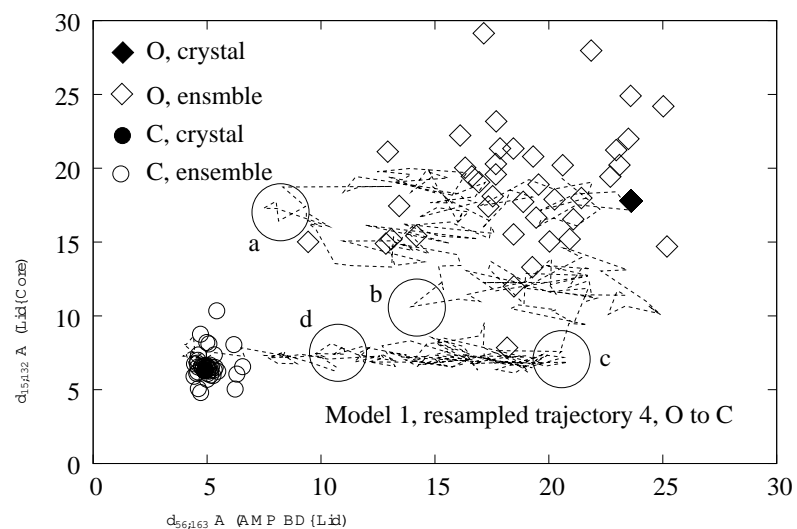


Figure 12: A resampled trajectory for the O to C transition obtained using Model 1 is shown via interresidue distance between pair of residues in the core and the flexible lid (ordinate) versus the distance between pair of residues in the AMP binding domain and the flexible lid (abscissa). The circles and the associated numbers represent the representative structures that are depicted in Figure 17.

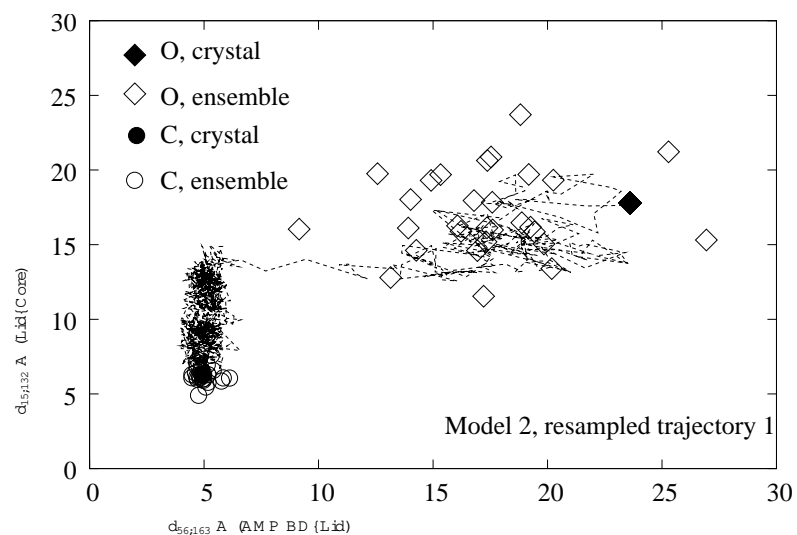


Figure 13: A resampled trajectory for the O to C transition obtained using Model 2 is shown via interresidue distance between pair of residues in the core and the flexible lid (ordinate) versus the distance between pair of residues in the AMP binding domain and the flexible lid (abscissa).

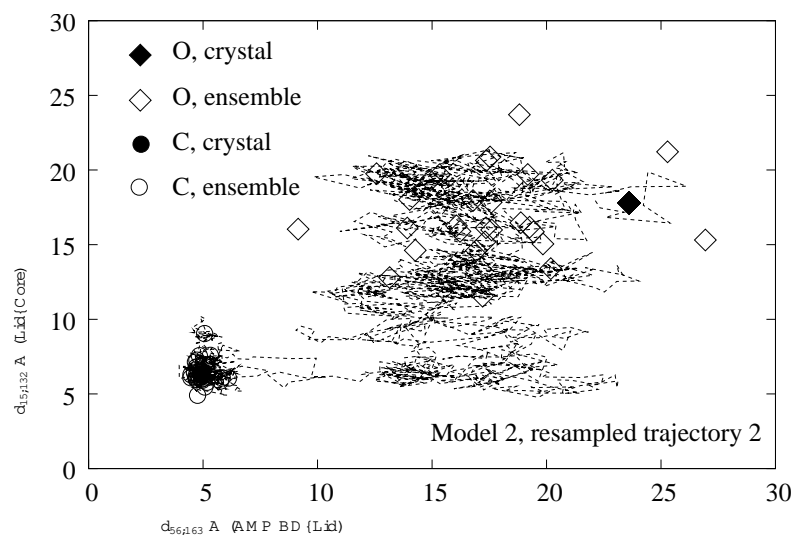


Figure 14: A resampled trajectory for the O to C transition obtained using Model 2 is shown via interresidue distance between pair of residues in the core and the flexible lid (ordinate) versus the distance between pair of residues in the AMP binding domain and the flexible lid (abscissa).

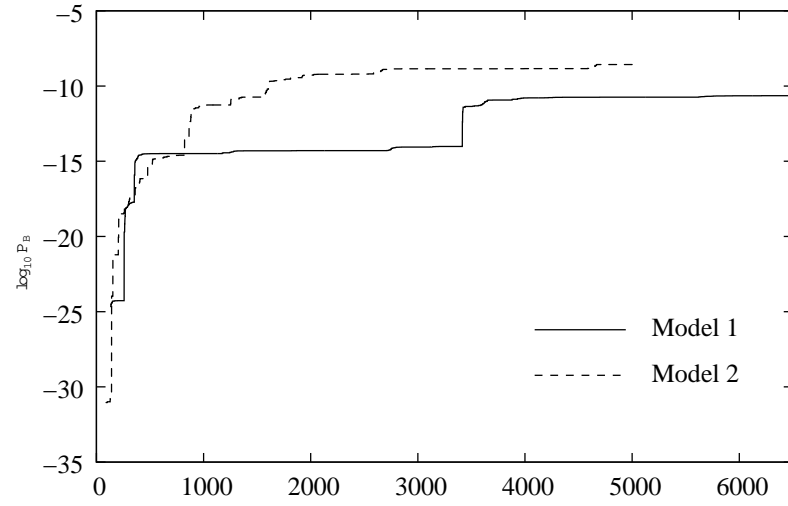


Figure 15: Probability flux into the O state as a function of WE snapshots (each snapshot is 2000 LBM C steps). The solid line is for Model 1, whereas the dashed line is for Model 2.

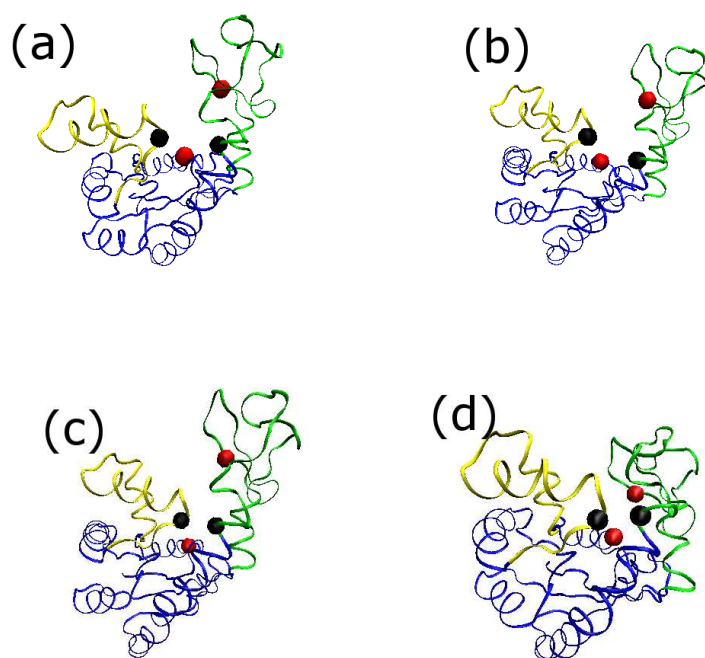


Figure 16: Representative structures along the transition path (Pathway 2) obtained in Figure 11 for Model 1.

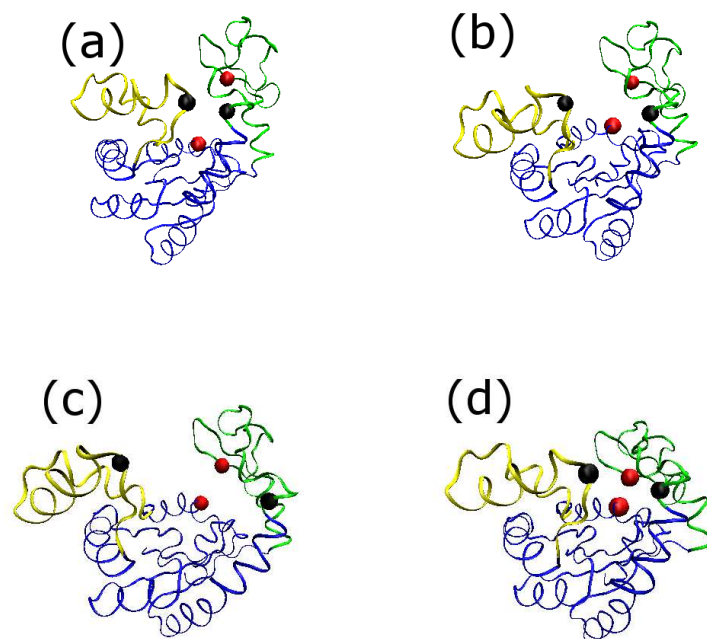


Figure 17: Representative structures along the transition path (Pathway 1) obtained in Figure 12 for Model 1.

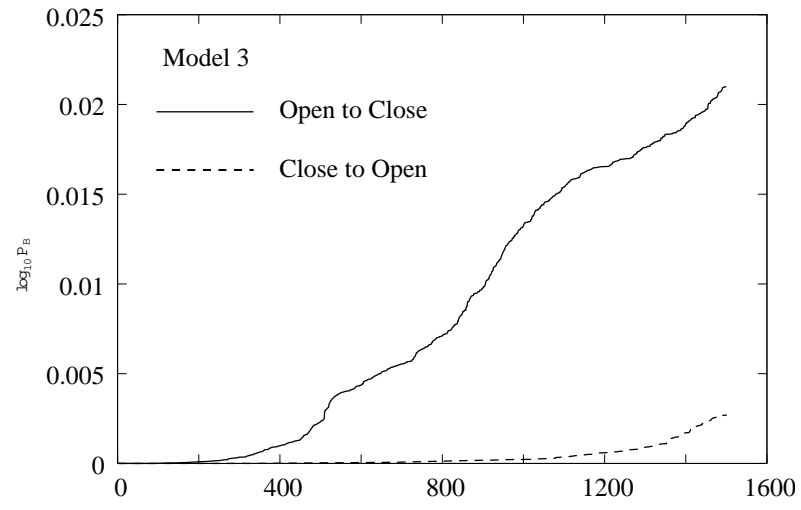


Figure 18: Probability flux in either direction for Model 3 as a function of W E snapshots (each snapshot is 2000 LBM C steps).